ACS APPLIED MATERIALS & INTERFACES

Research Article

www.acsami.org

Energy Storage in Ferroelectric Polymer Nanocomposites Filled with Core–Shell Structured Polymer@BaTiO$_3$ Nanoparticles: Understanding the Role of Polymer Shells in the Interfacial Regions

Ming Zhu,[†] Xingyi Huang,*[,†] Ke Yang,[†] Xing Zhai,[†] Jun Zhang,[†] Jinliang He,[‡] and Pingkai Jiang[†,§]

[†]Department of Polymer Science and Engineering, Shanghai Key Laboratory of Electrical Insulation and Thermal Aging, Shanghai Jiao Tong University, Shanghai 200240, China

[‡]State Key Lab of Power system, Department of Electrical Engineering, Tsinghua University, Beijing 100084, China

[§]Shanghai Engineering Center for Material Safety of Nuclear Power Equipment, Shanghai 200240, China

Supporting Information

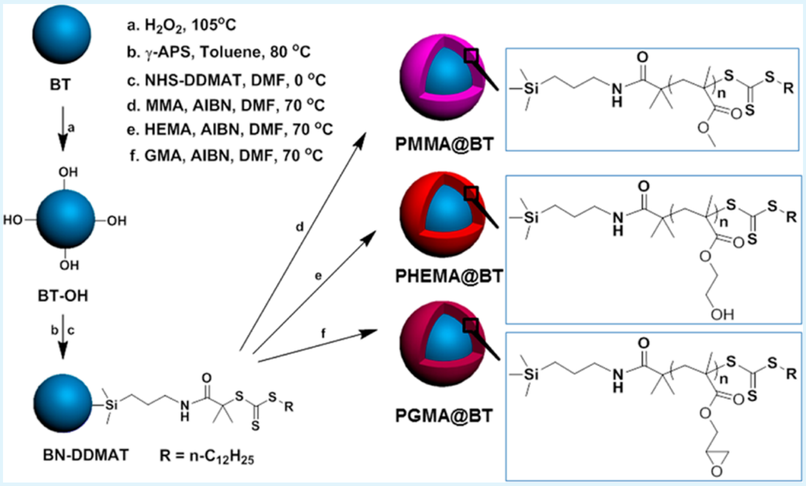

ABSTRACT: The interfacial region plays a critical role in determining the electrical properties and energy storage density of dielectric polymer nanocomposites. However, we still know a little about the effects of electrical properties of the interfacial regions on the electrical properties and energy storage of dielectric polymer nanocomposites. In this work, three types of core–shell structured polymer@BaTiO$_3$ nanoparticles with polymer shells having different electrical properties were used as fillers to prepare ferroelectric polymer nanocomposites. All the polymer@BaTiO$_3$ nanoparticles were prepared by surface-initiated reversible-addition–fragmentation chain transfer (RAFT) polymerization, and the polymer shells were controlled to have the same thickness. The morphology, crystal structure, frequency-dependent dielectric properties, breakdown strength, leakage currents, energy storage capability, and energy storage efficiency of the polymer nanocomposites were investigated. On the other hand, the pure polymers having the same molecular structure as the shells of polymer@BaTiO$_3$ nanoparticles were also prepared by RAFT polymerization, and their electrical properties were provided. Our results show that, to achieve nanocomposites with high discharged energy density, the core–shell nanoparticle filler should simultaneously have high dielectric constant and low electrical conductivity. On the other hand, the breakdown strength of the polymer@BaTiO$_3$-based nanocomposites is highly affected by the electrical properties of the polymer shells. It is believed that the electrical conductivity of the polymer shells should be as low as possible to achieve nanocomposites with high breakdown strength.

KEYWORDS: *dielectric constants, breakdown strength, core–shell nanoparticles, energy storage, nanocomposite, reversible-addition–fragmentation chain transfer (RAFT) polymerization, poly(vinylidene fluoride)*

INTRODUCTION

Dielectric materials with high dielectric constant, high breakdown strength, and low dielectric loss have important applications in electric energy storage devices such as capacitors.[1,2] Dielectric polymers not only have high breakdown strength and low dielectric loss but also have excellent flexibility and ease of processing and thus are excellent candidates for dielectrics of energy storage devices.[3,4] However, their low dielectric constant leads to low capability of energy storage.[5] Therefore, the increase of dielectric constant and

Received: July 7, 2014
Accepted: November 3, 2014
Published: November 3, 2014

meanwhile preserving other excellent electrical (e.g., high breakdown strength and low dielectric loss), mechanical (e.g., flexibility), and processing properties of the polymers are highly desirable for improving the capability of energy storage. So far, many strategies have been reported to increase the dielectric constant of the polymers.[6] Among them, the organic−inorganic hybrid strategy, namely, introducing high dielectric constant nanoparticles into a polymer matrix, has been widely adopted because this method usually does not cause significant increase of dielectric loss and large decrease of breakdown strength.[7−17]

Despite the promising potential of the organic−inorganic hybrid strategy, the unique physicochemical properties (e.g., large surface energy) of nanoparticles inevitably cause aggregation and inhomogeneity in the polymer matrix,[10] particularly in the case of high nanoparticle loading. It has been well recognized that the aggregation and inhomogeneity of nanoparticles are the main reasons resulting in deteriorated electrical properties in polymer nanocomposites. Surface modification and functionalization are effective to improve the nanoparticle−polymer compatibility, resulting in homogeneous dispersion of nanoparticles and thus significantly enhanced electrical properties. A variety of work has been devoted to improve the nanoparticle−polymer compatibility by engineering the nanoparticle surfaces.[18−24] Typical modifiers used to engineer the nanoparticle surfaces include silane coupling agents,[25] phosphonates,[20,21] and catechols (e.g., dopamine).[26] Taking barium titanate ($BaTiO_3$, hereafter referred to as BT) as a typical example, the effects of the nanoparticle modification and functionalization on the electrical properties and energy storage of polymer nanocomposites have been well documented. For instance, the work of Perry et al. reported that the poly(vinylidene fluoride-*co*-hexafluoro propylene) [P(VDF-HFP)] nanocomposites filled with phosphonic acid modified BT exhibit a remarkable combination of high dielectric constant and high breakdown strength and thus a high energy storage capability.[20]

More recently, the preparation of core−shell structured high dielectric constant nanoparticles by surface-initiated in situ polymerization has received a lot of interest.[1,7,10,27−38] The main merit of this method is that the nanoparticles are well encapsulated by desirable polymers, which can significantly improve the nanoparticle dispersion in a polymer matrix and result in improved electrical properties of the polymer nanocomposites. Our groups have been devoted to this method for years and prepared several kinds of high dielectric constant polymer/BT nanocomposites for dielectric and energy storage application via "grafting from" or "grafting to" methods.[33−38] In addition, the effects of the shell/matrix interactions on the electrical properties and energy storage of the nanocomposites were also demonstrated in a recent publication.[36] It has been found that, when the polymer shells have similar electrical properties, a strong shells/matrix interaction is helpful to suppress the dielectric loss and enhance the energy storage capability.[36] These results provide important information for the further development of the dielectric polymer nanocomposites for dielectric and energy storage applications.

For further optimizing the energy storage of core−shell nanoparticles based polymer nanocomposites, it is of importance to know the role of the electrical properties of the polymer shells in determining the electrical properties and energy storage of the nanocomposites. This can help us to design and realize the desirable interface in the nanocomposites. In this work, by using reversible-addition−fragmentation chain transfer (RAFT) polymerization, three kinds of core@shell nanoparticles with polymer shells having different electrical properties were synthesized. The effects of the electrical properties of the polymer shells on the electrical properties and energy storage of the core@shell nanoparticles based PVDF nanocomposites were investigated. Our results show that the energy storage capability, energy storage efficiency, and breakdown strength of the core−shell nanoparticles based nanocomposites can be tailored by adjusting the electrical properties of the polymer shells of the core−shell nanoparticles.

■ EXPERIMENTAL SECTION

Materials. BT nanoparticles with an average diameter of about 100 nm were provided by the Shandong Sinocera Functional Material Company, China. The polyvinylidene fluoride (PVDF, 6010) was provided by Solvay Shanghai Co., China. Methyl methacrylate (MMA), hydroxyethyl methacrylate (HEMA), and glycidyl methacrylate (GMA) were supplied by Aladdin. An aqueous solution of H_2O_2 (30 wt %), *N*,*N*-dimethylformamide (DMF), dichloromethane (DCM), toluene, and other organic reagents or solvents was supplied by Shanghai Reagents Co. Ltd. *N*-Hydroxysuccinimide (NHS), *N*,*N*′-dicyclohexylcarbodiimide (DCC), 4-dimethylaminopyridine (DMAP), and γ-aminopropyl triethoxysilane (γ-APS) were purchased from Acros. The MMA, HEMA, and GMA monomers were passed through a basic alumina column before use. All other chemicals were used as received except for special notes. The RAFT agent *S*-1-dodecyl-*S*′-(α,α′-dimethyl-α″-acetic acid) thrithiocarbonate (DDMAT) was synthesized according to the literature.[39]

Functionalization of the BT Nanoparticles. The activation of a RAFT agent (DDMAT-NHS) was according to the literature.[40] The surface modification of the original BT nanoparticles was as follows:

The ***first*** step was hydroxylation and amino functionalization of BT nanoparticles. Briefly, 10 g of $BaTiO_3$ and 100 mL of H_2O_2 (30 wt %) were mixed in a three-necked round-bottom flask. After sonication for 30 min, the mixture was heated to 80 °C for 2 h and refluxed at 105 °C for 4 h with stirring. The nanoparticles were washed with deionized water and collected by centrifuging for 5 min at 8000 rpm. Then they were dried under vacuum at 80 °C for 24 h and named as BT-OH. To obtain the amino-functionalized BT (BT-HN_2), 10 g of BT-OH and 80 mL of toluene were put in a round-bottom flask and sonicated for 30 min to disperse. Then 5 g of γ-APS was added, and the mixture was stirred at 80 °C for 24 h. The nanoparticles were obtained by centrifugation at 8000 rpm for 5 min and washed with toluene twice.

The ***second*** step was the preparation of DDMAT anchored BT. An amount of 10 g of BT-NH_2 was dispersed in DMF and sonicated for 30 min, and then the mixture was added dropwise to the DCM solution of NHS-EDMAT at 0 °C with vigorous stirring. The mixed solution was reacted at 0 °C for 6 h and 25 °C for 12 h. After reaction, the BT-DDMAT was obtained by centrifugation and washed with toluene twice. Then the BT-DDMAT was dried at 60 °C for 24 h.

The ***third*** step was the preparation of polymer@BT nanocomposites via RAFT surface-initiated polymerization from BT-DDMAT. Three different monomers were successfully grafted to the surface of BT to obtain core−shell structure (PMMA@BT, PHEMA@BT, and PGMA@BT). The typical procedures were as follows: BT-DDMAT (1.00 g, 0.0164 mmol), RAFT agent DDMAT (2.98 mg, 0.0082 mmol), DMF (6 mL), and MMA (3.0 g) were mixed into a 50 mL round-bottom flask followed by sonication and addition of AIBN (1.21 mg, 0.007 mmol). The flask was sealed with a rubber plug and followed by deoxygenation by purging nitrogen gas for 30 min. The flask was immersed into an oil bath at 70 °C with magnetic stirring, and after reaction for 12 h, the flask was cooled to room temperature and opened to the air. The solution was diluted with $CHCl_3$, then centrifuged to decant the supernatant, and washed by acetone three times. The products were dried under vacuum at 60 °C for 24 h. The synthesis of the BT@PHEMA and BT@PGMA was similar except for the reaction time and that the BT@PHEMA was washed by DMF.

Scheme 1. Scheme Illustrating the Preparation Process of the Polymer@BT Nanoparticles by Surface-Initiated RAFT Polymerization

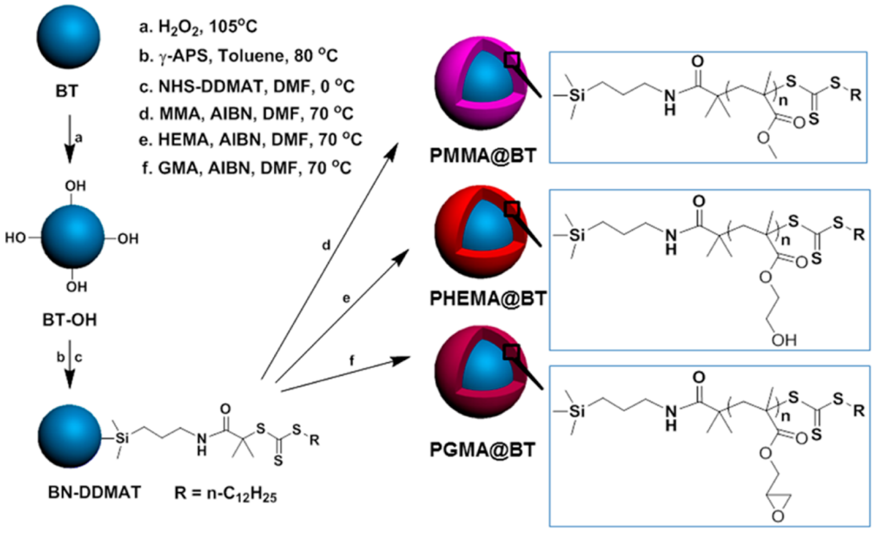

Preparation of Polymer@BT/PVDF Nanocomposite Films. The preparation of polymer@BT/PVDF composite films was conducted as follows: polymer@BT was dispersed in DMF and sonicated for 30 min; meanwhile, PVDF was dissolved in DMF and stirred for 30 min. Then the solution of polymer@BT was dropped into the PVDF solution slowly and sonicated for another 30 min. The mixture was stirred overnight. After that, the solution was dripped to a silicon plate and heated to 100 °C to remove the solvent. The preliminary film was dried under vacuum at 80 °C and then was molded by hot-pressing at 180 °C for 5 min. The thickness of the films was 30−50 μm.

Characterization. The ^{1}H NMR spectra of all samples were tested by a Varian Mercury Plus 400-MHz spectrometer in $CDCl_3$, except for PHEMA samples in CD_3OD, and TMS was used as the standard. Fourier transform infrared (FT-IR) spectroscopy over the range of 4000−450 cm^{-1} was conducted with a PerkinElmer Paragon 1000 instrument. Thermogravimetric analysis (TGA) of modified $BaTiO_3$ nanoparticles by a NETZSCH TG209 F3 instrument was performed at a heating rate of 20 °C min^{-1} (50−800 °C) in nitrogen flow (20 mL min^{-1}). Differential scanning calorimetry (DSC) characterization of nanocomposites was conducted under nitrogen atmosphere at a heating/cooling rate of 10 °C min^{-1} between 20 and 200 °C by using a NETZSCH 200 F3 instrument. The X-ray diffraction pattern (XRD) spectra were measured from 20 to 80 °C at the rate of 5°C/min in a Rigaku D/max-2200/PC diffractometer. The samples were annealing at 120 °C for 24 h before being tested. Scanning electron microscopy (SEM) images of the cross section were recorded by a field emission scanning electron microscope (Nova NanoSEM 450, FEI, America). Samples were fractured in liquid nitrogen. Transmission electron microscopy (TEM) images of core−shell structured nanoparticles were operated by a JEOL JEM-2100 instrument at an accelerating voltage of 160 kV. Samples were prepared by dropping the sample solutions onto carbon-coated cooper grids and air-dried before measurement. A Novocontrol Alpha-N high resolution dielectric analyzer (GmbH Concept 40) was used to characterize the dielectric properties of all the nanocomposites with frequency range 10^{-1}−10^6 Hz. A layer of gold was evaporated on both surfaces to serve as electrodes. Electric displacement−electric field (*D*−*E*) loops were carried out at 100 Hz and room temperature by a Precision Premier II ferroelectric polarization tester (Radiant, Inc.). Samples were sputtered by gold with diameter of 3 mm on both sides as electrodes. Only the samples having thickness of about 40 μm were selected for breakdown measurements. The DC breakdown strength was taken by using a dielectric strength tester with 10 mm ball to ball electrode (DH, Shanghai Lanpotronics Co., China).

■ RESULTS AND DISCUSSION

Preparation and Characterization of Polymer@BT Nanoparticles. Scheme 1 illustrates the preparation process of the core−shell structured polymer@BT nanoparticles by surface-initiated RAFT polymerization. The RAFT agent DDMAT was activated by NHS before being anchored to the surfaces of the BT nanoparticles. This process was used to avoid the aminolysis of the thioester group by the reaction with amino groups.[37,40] The ^{1}H NMR spectra were used to prove the successful activation of DDMAT. As shown in Figure S1 in the Supporting Information, a new proton signal peak at 2.81 ppm appears in the ^{1}H NMR spectrum of DDMAT-NHS. Surface modification of the BT nanoparticles was first investigated by FT-IR measurement (see Figure 1). Compared with the BT-OH, a new absorption band of −Si−O− at 1080 cm^{-1} was observed in the BT-NH_2, indicating the successful introduction of the silane coupling agent. In the case of BT-DDMAT, the strong peaks at 2920 and 2853 cm^{-1} appear, which should be attributed to the asymmetric and symmetric stretching vibrations of −CH_2−. The attachment of DDMAT onto the surfaces of the BT nanoparticles is further confirmed

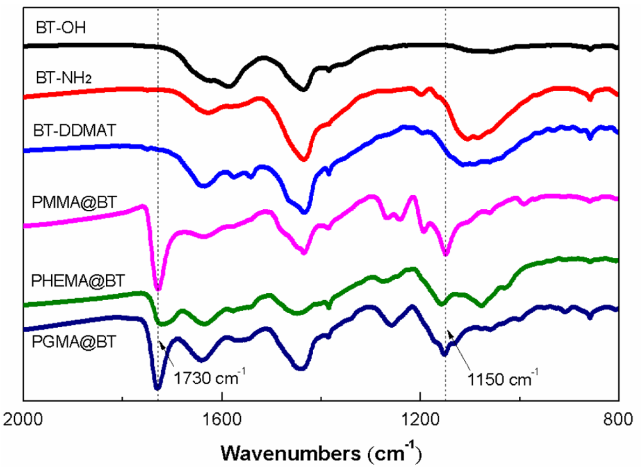

Figure 1. FT-IR spectra of the functionalized BT nanoparticles.

by the ^{1}H NMR spectra. As shown in Figure S2 in the Supporting Information, the proton signals of $-CH_3$ and $-CH_2-$ in BT-DDMAT correspond to the ^{1}H NMR spectrum of DDMAT.

The BT nanoparticles functionalized via surface-initiated RAFT polymerization were characterized by FTIR and ^{1}H NMR spectra. One can see from Figure 1 that, compared with the FT-IR spectrum of BT-DDMAT, new absorption peaks at 1730 and 1140 cm^{-1} appear in the spectra of the functionalized nanoparticles via RAFT polymerization, which should be attributed to the stretching vibrations of the C═O and C−O groups of polymer chains grafted onto the nanoparticle surfaces. In the case of ^{1}H NMR spectra (see Figures S3 and S4 in the Supporting Information), MMA-, HEMA-, and GMA-functionalized BT nanoparticles by RAFT have similar proton signal peaks with PMMA, PHEMA, and PGMA, respectively, indicating that PMMA, PHEMA, and PGMA have been successfully grafted onto the surfaces of the BT nanoparticles. The TGA curves provide further evidence for the successful grafting of polymers onto the BT nanoparticle surfaces. One can see from Figure 2 that the weight loss of the nanoparticles shows the order of BT-OH < BT-NH$_2$ < BT-DDMAT < polymer@BT. In addition, all the polymer@BT nanoparticles show a similar weight loss (around 4%), indicating that the polymer shells have a similar thickness, which will be further confirmed in the following TEM analysis.

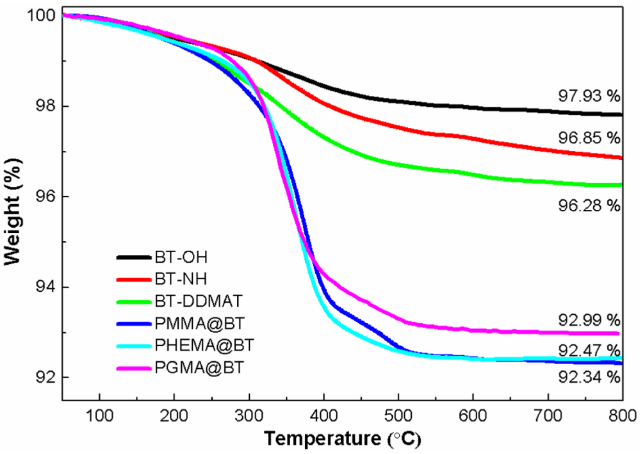

Figure 2. TGA curves of the functionalized BT nanoparticles.

TEM was used to observe the morphology of the functionalized BT nanoparticles via RAFT polymerization. Figure 3 shows the TEM images of PMMA-, PHEMA-, and PGMA-grafted BT nanoparticles. One can see that, in each case, the BT nanoparticles are homogeneously encapsulated by a layer of polymer. The thickness of each polymer layer is nearly the same and is about 2−3 nm, which is consistent with the calculated values according to the grafted polymer weight derived from the TGA curves and the specific surface area of the BT nanoparticles.

Microstructure of the Polymer@BT-Based Nanocomposites. Figure 4 shows the SEM images of the fractured cross sections of the polymer@BT-based PVDF nanocomposites. One can see from Figure 4 that the three nanocomposites have similar microstructure. Namely, each nanocomposite is mainly composed of particulates, and the polymer matrix cannot be recognized easily. In other words, it seems that the volume fractions of the particulates are much higher than 20%. Such an observation can only be understood by such an explanation that the PVDF matrix has excellent compatibility with the polymer shells, resulting in PVDF encapsulated polymer@BT (here, the polymers refer to PMMA, PHEMA, PGMA) core−shell morphology in the nanocomposites. The excellent miscibility of PVDF and PMMA has been well-known, which should be attributed to the strong dipole−dipole interactions between the carbonyl groups in PMMA chains and fluorine atoms in PVDF chains.[41] The hydroxyl groups of PHEMA and the epoxy groups in PGMA further enhance dipole−dipole interactions of PVDF/PHEMA and PVDF/PGMA systems, respectively, resulting in good compatibility of PVDF/PHEMA and PVDF/PGMA. In addition, the hydrogen bonding (—F···H—O—) between strong electronegative element F in the PVDF chains and the hydroxyl groups of PHEMA should also enhance the compatibility of PVDF/PHEMA.[42]

PVDF is a ferroelectric polymer, which has a complex structure and exhibits five crystalline phases, in which α, β, and γ are the most possible phases.[42] The β-phase is technically important because it has the largest dipolar moment, not only resulting in high dielectric constant but also leading to high electroactivity.[43] Therefore, it is of importance to know the effects of polymer@BT nanoparticles on the structure of the PVDF matrix. XRD and FT-IR techniques were used to obtain the structure information on PVDF in nanocomposites. It has been summarized in previous work[42] that the peaks of 1276 and 840 cm^{-1} indicate the β-phase of PVDF, whereas the absorption bands at 762, 794, 855, and 970 cm^{-1} indicate the α-phase of PVDF. Figure 5 shows the FT-IR ATR spectra of the polymer@BT/PVDF nanocomposites. Each nanocomposite exhibits the characteristic absorption bands of α- and β-phases, indicating the PVDF matrix is composed of these two phases in the nanocomposites. These results are further identified by the XRD curves of the nanocomposites. As shown in Figure 6, each nanocomposite shows the character-

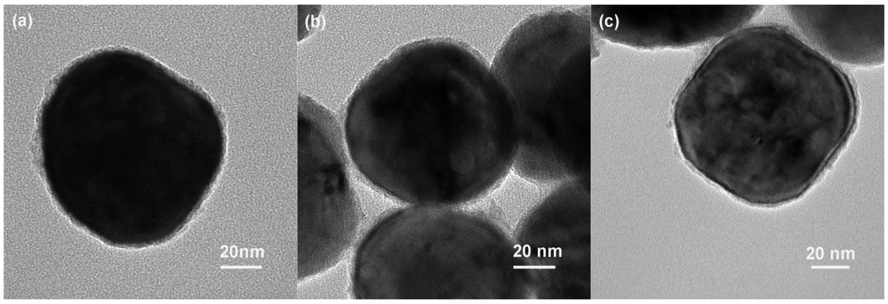

Figure 3. TEM images of PMMA (a), PHEMA (b), and PGMA (c) functionalized BT nanoparticles via RAFT polymerization.

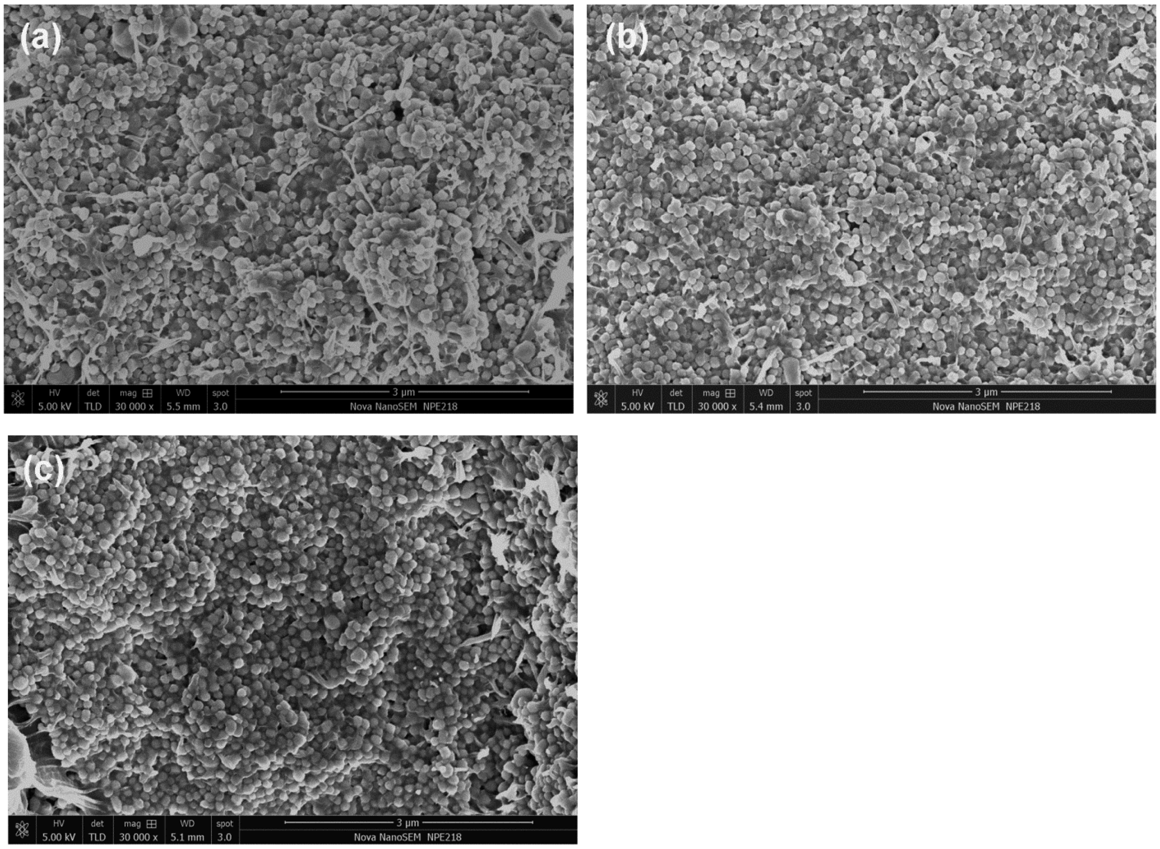

Figure 4. SEM images of the polymer@BT-based PVDF nanocomposites: (a) PMMA@BT/PVDF, (b) PHEMA@BT/PVDF, and (c) PGMA@BT/PVDF. All samples contain 20 vol % polymer@BT nanoparticles.

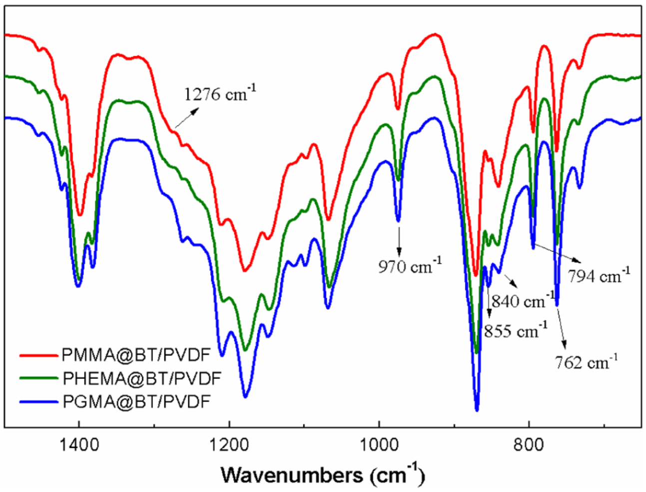

Figure 5. FT-IR spectra of polymer@BT-based PVDF nanocomposites.

istic diffractograms of the β-phase at $2\theta = 20.26°$ corresponding to the (110) plane and α-phase at $2\theta = 17.66°$ and 18.30° corresponding to the diffractions in planes (100), (020), and (110), respectively.[42,43]

Dielectric Properties of the Polymer Shells from the Polymer@BT Nanoparticles. One of the core aims of this work is to explore the role of polymer shells in determining the dielectric properties and energy storage of the polymer@BaTiO$_3$-based nanocomposites. In order to achieve deep insights into this issue, it is necessary to know the dielectric properties of the polymer shells from the polymer@BaTiO$_3$ nanoparticles. Figure 7 shows the frequency-dependent dielectric properties of the free shell polymers prepared via in situ RAFT polymerization. It can be seen from Figure 7 that (i) PMMA and PGMA show similar dielectric response (i.e., β relaxation[34]) although PMMA has a longer relaxation time; (ii) PHEMA shows an apparent interfacial polarization (e.g., electrode polarization),[44,45] resulting in significantly enhanced low frequency dielectric constant and dielectric loss; (iii) compared with PMMA and PGMA, PHEMA has the highest dielectric constant and the highest dielectric loss over the whole measurement frequency range; and (iv) PGMA shows a higher

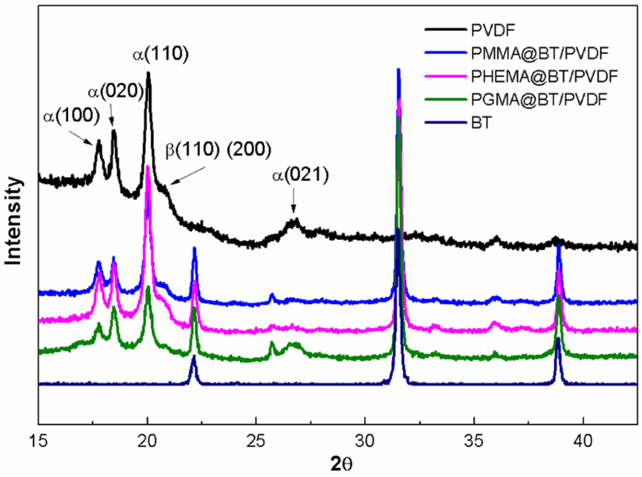

Figure 6. XRD curves of polymer@BT-based PVDF nanocomposites.

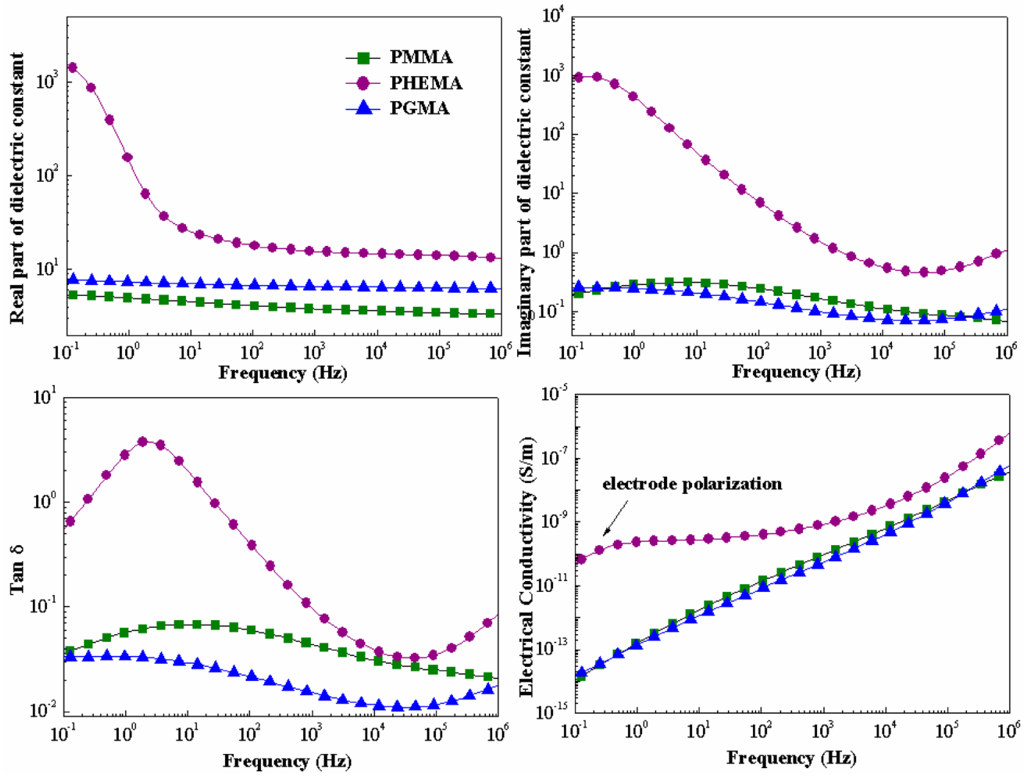

Figure 7. Frequency dependence of dielectric properties for polymer shells of the polymer@BT nanoparticles.

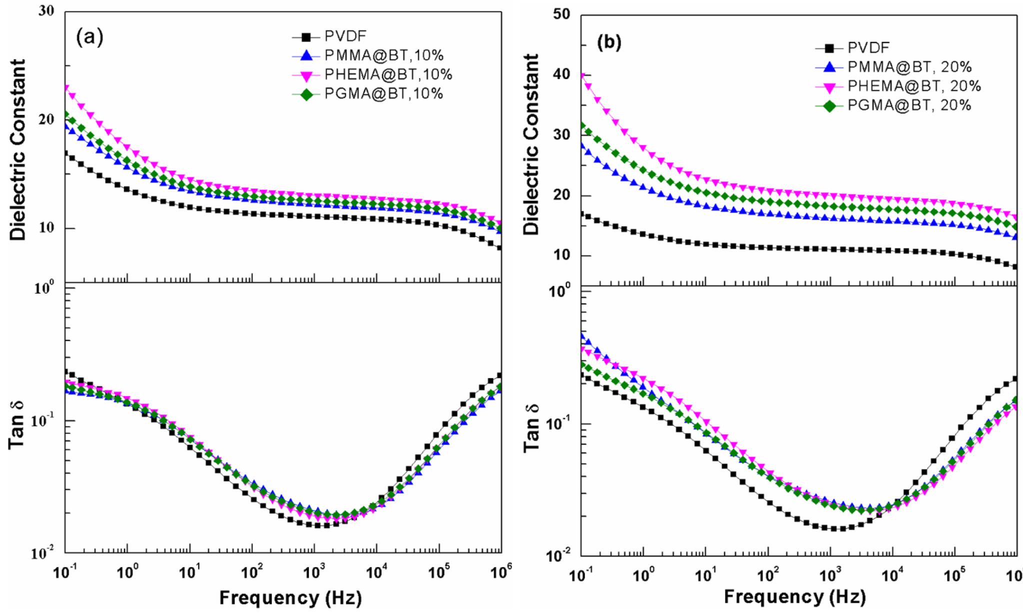

Figure 8. Frequency dependence of dielectric constant and dielectric loss tangent of the polymer@BT-based PVDF nanocomposites. (a) 10 vol % BT and (b) 20 vol % BT.

dielectric constant in comparison with PMMA but has the minimum dielectric loss among the three polymers, exhibiting desirable dielectric properties for power energy storage applications.[1,6] The difference among the dielectric properties of the three polymers should be attributed to the different dipole moment of pendant groups.[46] The pendant hydroxyethyl groups have the large dipole moment, which results in the highest dielectric constant of the PHEMA. The high dielectric loss and high dielectric constant of PHEMA, particularly at low frequencies, should be mainly attributed to its moisture absorption caused by its strong hydrophilicity.

Dielectric Properties of the Polymer@BT-Based PVDF Nanocomposites. Figure 8 shows the frequency-dependent dielectric constant and dielectric loss tangent of the polymer@BT/PVDF nanocomposites at room temperature. One can see from Figure 8 that, compared with the PVDF matrix, all the nanocomposites show enhanced dielectric constants. However, the dielectric constant enhancement is marginal at low

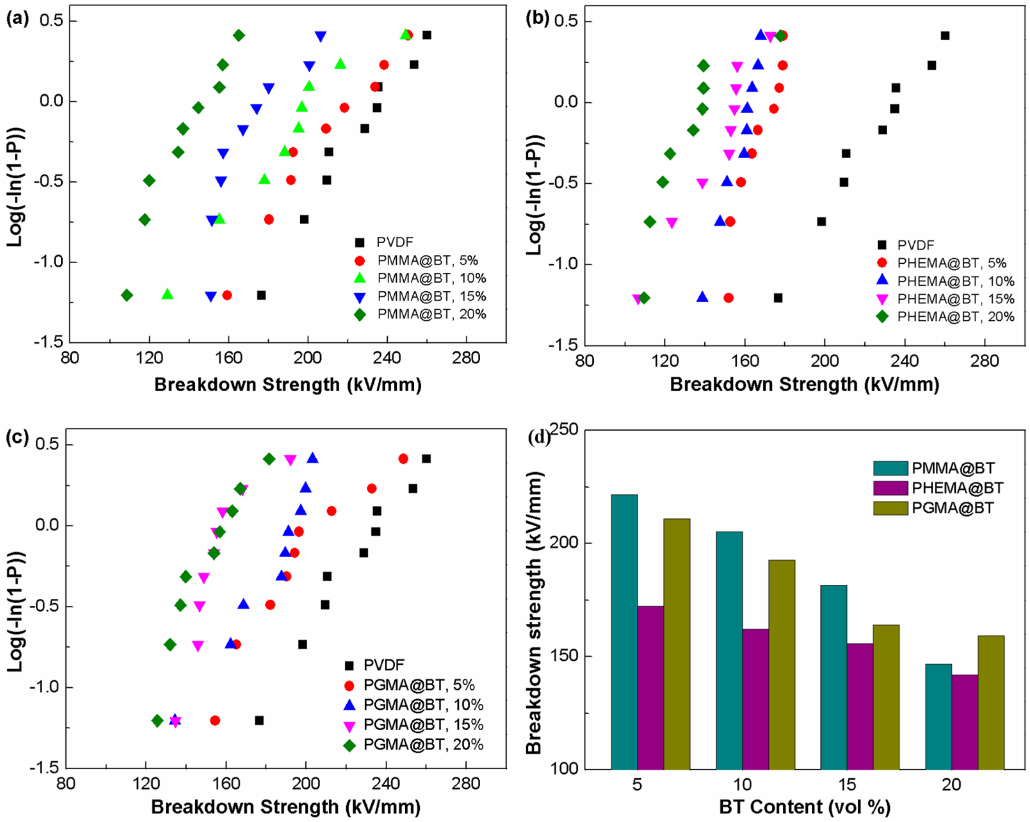

Figure 9. Weibull plots of breakdown strength (a, b, c) and characteristic breakdown strength (d) of the polymer@BT-based PVDF nanocomposites.

polymer@BT loading (i.e., 10 vol %). When the loading of polymer@BT is high (e.g., 20 vol %), the dielectric constant enhancement becomes significant. For instance, when the polymer@BT loading is 20 vol %, the dielectric constant of the nanocomposites at 1000 Hz increases to 20.2 for PHEMA@BT/PVDF from 10.9 of the pure PVDF. The dielectric constant enhancement or the dielectric constants of the nanocomposites follow the order of PHEMA@BT/PVDF > PGMA@BT/PVDF > PMMA@BT/PVDF, which are consistent with the case of the polymer shells shown in Figure 7. This result indicates that, at the same BT content, the dielectric constants of the nanocomposites are determined by the dielectric constants of the interfacial region. That is, the high-dielectric-constant interfacial region tends to result in high dielectric constants of the nanocomposites. Unlike the free polymers in which different frequency dependence of dielectric constant was observed (Figure 7), all the nanocomposites have a similar frequency dependence of dielectric constant with the pure PVDF. This may be understood by two factors. One is the strong polymer@BT/PVDF interaction, which significantly suppresses the macromolecular movement in the interfacial region. The second is restricted dipole movement of grafted polymer chains

The differences in dielectric loss tangent between the nanocomposites and the pure PVDF are dependent on the polymer@BT loading, whereas the differences between different nanocomposites are marginal and independent of the loading of polymer@BT. As shown in Figure 8, when the loading of polymer@BT is low, the nanocomposites have the comparable dielectric loss tangent with the pure PVDF. At high loading, the introduction of the polymer@BT causes higher dielectric loss at low frequencies. In both cases, the high-frequency dielectric loss tangent of the nanocomposites is always lower than that of the pure PVDF. In fact, many previous works have reported that, in polar thermoplastic polymer composites with inorganic fillers,[35,47,48] the composites tend to exhibit lower dielectric loss tangent at high frequencies. One possible reason for this is that the inorganic fillers limit the macromolecular movement, which plays a role like “freezing”, thus resulting in low dielectric loss. Regarding the frequency dependence of loss tangents in Figure 8, it appears that the larger loading levels of the core−shell nanoparticles result in higher dielectric loss. This suggests that the friction (dissipation) for the reorientation of the matrix polymer chains increases with the loading of the core−shell polymer@BT nanoparticles.

It should be noted that the free PHEMA shows an apparent interfacial polarization (i.e., electrode polarization) peak in frequency dependence of dielectric loss tangent, but this peak disappears in the PHEMA@BT-based nanocomposites. Here, the appearance of electrode polarization in free PHEMA is because of the medium electrical conductivity of the PHEMA, which makes charges accumulate in the thin layers beneath the sample surface.[49] When PHEMA@BT nanoparticles were dispersed into the PVDF matrix, the PHEMA shell isolated by PVDF and the PHEMA shell cannot be interconnected with each other, resulting in the absence of the electrode polarization in the PHEMA@BT nanocomposites.

Breakdown strength, E_b, is an important electrical parameter for evaluating the potential power energy storage of the dielectric materials.[1,6] High breakdown strength is required for achieving the maximum energy density. This is because the

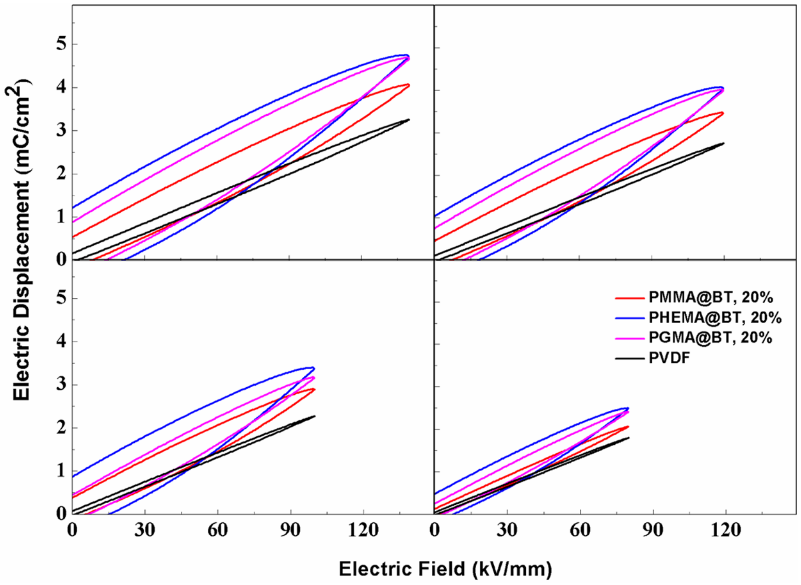

Figure 10. Electric displacement−electric field (D−E) loops and leakage currents of the polymer@BT-based PVDF nanocomposites.

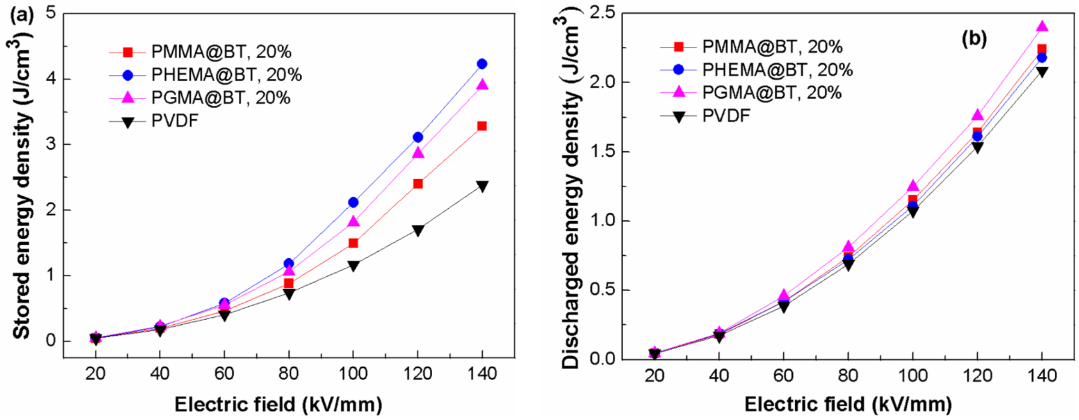

Figure 11. Stored (a) and discharged (b) energy densities of PVDF and polymer@BT-based PVDF nanocomposites.

maximum energy storage density $U_{\max}$ of a dielectric is determined by $U_{\max} = 1/2\varepsilon\varepsilon_0 E_b^2$, where ε and ε_0 are the dielectric constant of the dielectric and vacuum, respectively. In this work, the breakdown strength of the nanocomposites was evaluated by a two-parameter Weibull statistic distribution method, in which the cumulative probability of failure (i.e., electrical breakdown) P for a sample was expressed as[25,48]

$$P = 1 - \exp\left[-\left(\frac{E}{E_0}\right)^{\beta}\right] \tag{1}$$

where β is a parameter related to the scatter of the data, and E and E_0 are the experiment breakdown strength and the characteristic breakdown strength at the cumulative failure probability of 63.2%, respectively. E_0 has been used to represent the breakdown strength of dielectric materials. In our experiments, nine specimens were used to perform the breakdown measurements of one sample.

Figure 9 shows the Weibull plots of breakdown strength for the polymer@BT/PVDF nanocomposites. One can see from Figure 9 that, compared with PVDF, all the nanocomposites show decreased breakdown strength after the introduction of polymer@BT nanoparticles. In addition, the breakdown strength of each nanocomposite decreases with the increase of nanoparticle loading. The decrease of breakdown strength of the nanocomposites is mainly caused by the large electrical mismatch between the matrix and fillers.[1] Figure 9d summarizes the characteristic breakdown strength of every nanocomposite. Interestingly, the polymer shells of polymer@BT indeed play an important role in determining the breakdown strength of the nanocomposites. As shown in Figure 9d, the PHEMA@BT-based nanocomposites always have the lowest breakdown strength. The PMMA@BT-based nanocomposites have higher breakdown strength in comparison with the PGMA@BT/PVDF nanocomposites except the sample with 20% core−shell nanoparticles. Such results are generally consistent with the order of the shell dielectric constant of the polymer@BT nanoparticles. Namely, the nanocomposites with polymer@BT having a high dielectric constant shell have low breakdown strength. On the other hand, the high electric field induced ionization of the −OH groups from PHEMA may produce water molecules, which have high dielectric constant (i.e., 80), thus being an important factor causing significant reduction in breakdown strength of the PHEMA@BT/PVDF nanocomposites.

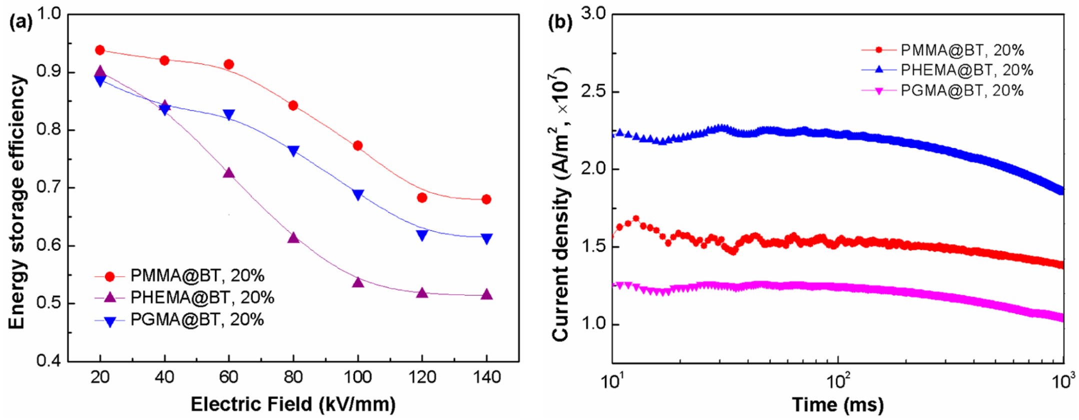

Figure 12. Energy storage efficiencies (a) and leakage currents (b) of the nanocomposites with 20 vol % BT nanoparticles. The leakage currents were measured under an electric field of 100 kV/mm.

Energy Storage of the Polymer@BT-Based PVDF Nanocomposites. The electric displacement−electric field ($D-E$) loops of every nanocomposite were measured, and the selected results of nanocomposites with 20 vol % polymer@BT are shown in Figure 10. One can see from Figure 10 that, among the nanocomposites, the PHEMA@BT-based nanocomposites have the highest electric displacement, the highest remnant polarization, and the highest leakage currents. In addition, their $D-E$ loops are wider than those of the others. The PMMA@BT-based nanocomposites have the lowest electric displacement and remnant polarization. The $D-E$ loops of the PMMA@BT-based nanocomposites are also narrower than those of the others.

The energy densities of the nanocomposites are provided in Figure 11, which were calculated according to the $D-E$ loops shown in Figure 10 by the equation of $U = \int EdD$, where E is the electric field and D is the electric displacement.

One can see from Figure 11 that the PHEMA@BT-based nanocomposites have the highest stored energy densities, whereas the PMMA@BT-based nanocomposites have the lowest. For example, at an electric field of 140 kV/mm, the stored energy densities of the PHEMA@BT/PVDF, PGMA@BT/PVDF, and PMMA@BT/PVDF are 4.23, 3.90, and 3.28 J/cm^3, respectively. This is because, under a given electric field, the storage energy is mainly determined by the electric displacement or dielectric constant. The discharged energy density, a more important parameter to characterize the effective energy storage capability of dielectric materials,[29,30] exhibits a different order among the nanocomposites. The PGMA@BT-based nanocomposites have the highest discharged energy densities, and the PHEMA@BT-based nanocomposites have the lowest. For instance, at an electric field of 140 kV/mm, the discharged energy densities of the PHEMA@BT/PVDF, PMMA@BT/PVDF, and PGMA@BT/PVDF are 2.18, 2.24, and 2.40 J/cm^3, respectively. This result indicates that the discharged energy densities are not only determined by the electric displacement/dielectric constant but also associated with the remnant polarization.

The energy storage efficiency, Eff_U, which is defined as the capability to release the stored energy, is calculated by

$$\mathrm{Eff}_U = \frac{U_{\mathrm{discharged}}}{U_{\mathrm{stored}}} \tag{2}$$

where $U_{\mathrm{discharged}}$ and U_{stored} represent the discharged and stored energy densities, respectively. The energy storage efficiencies of the nanocomposites are shown in Figure 12. One can see that the efficiencies show the order of PMMA@BT/PVDF > PGMA@BT/PVDF > PHEMA@BT/PVDF. Figure 12 also provides the leakage currents of the nanocomposites, which show the order of PGMA@BT/PVDF < PMMA@BT/PVDF > PHEMA@BT/PVDF. At high electric fields, the dielectric loss of dielectric materials is mainly determined by the leakage currents.[9] The higher leakage currents in PHEMA@BT-based PVDF nanocomposites (Figure 12b) widen the $D-E$ loops,[26,50] resulting in higher remnant polarization and low energy storage efficiency. The widening or narrowing of $D-E$ loops may be partially associated with the intrinsic dipolar moment variation of the PVDF matrix. In the case of pure PVDF, electric field induced dipolar orientation is the main origin of remnant polarization.[51] Therefore, the interactions between the PVDF matrix and the core−shell nanoparticles may affect the remnant polarization of PVDF in the PHEMA@BT-based nanocomposites. However, the final influence on remnant polarization of the PHEMA@BT-based nanocomposites should be marginal since the nanocomposites exhibit much higher remnant polarization in comparison with the pure PVDF, as shown in Figure 10.

■ CONCLUSIONS

We have prepared ferroelectric polymer nanocomposites using core−shell structured polymer@BaTiO$_3$ nanoparticles as fillers. Three kinds of polymer@BaTiO$_3$ nanoparticles (i.e., PMMA@BT, PGMA@BT, and PHEMA@BT) with the shells having different electrical properties were prepared by surface-initiated RAFT polymerization. We have investigated the effects of the polymer shells on the morphology, crystal structure, frequency-dependent dielectric properties, breakdown strength, leakage currents, energy storage capability, and energy storage efficiency of the nanocomposites. In order to get deep insights into the role of the polymer shell in determining the electrical properties and energy storage of the nanocomposites, the polymers (i.e., PMMA, PGMA, and PHEMA) having the same molecular structure with the shells were also prepared by RAFT polymerization, and their dielectric properties were also investigated.

The core−shell nanoparticles with high dielectric constant shells can result in high electric displacement and thus high energy densities in the nanocomposites, but the high leakage currents cause high dielectric loss and low discharged energy densities in the nanocomposites. In addition, the high dielectric constant polymer shells have high electrical conductivity, causing significant decrease of breakdown strength and thus poor maximum-energy-storage capabilities. The nanocomposites filled with core−shell nanoparticles having low dielectric constant shell show low electric displacement and thus low energy densities, but the low leakage currents cause low dielectric loss and thus high discharged energy density. Therefore, the optimum case is that the polymer shells have the combination of high dielectric constant and low leakage currents, which make the nanocomposites not only have high discharged energy densities but also have high energy efficiency.

■ ASSOCIATED CONTENT

Ⓢ Supporting Information

^{1}H NMR spectra of DDMAT, DDMAT-NHS, BT-DDMAT, PMMA, PHEMA, PGMA, PMMA@BT, PHEMA@BT, and PGMA@BT. This material is available free of charge via the Internet at http://pubs.acs.org.

■ AUTHOR INFORMATION

Corresponding Author

*E-mail: xyhuang@sjtu.edu.cn.

Author Contributions

X.Y.H. conceived the idea of the work. M.Z. prepared the samples and performed the FTIR, XRD, SEM, TEM, TGA, dielectric spectroscopy, breakdown strength, and properties measurements. The measurement of $D-E$ loops was performed by K.Y., and X.Z performed the NMR measurement. X.Y.H. wrote the manuscript. All authors commented on the manuscript.

Notes

The authors declare no competing financial interest.

■ ACKNOWLEDGMENTS

X.Y.H. thanks the SMC Excellent Young Faculty Award of Shanghai Jiao Tong University, Shanghai Pujiang Program under Grant PJ14D018, the National Natural Science Foundation of China (Nos. 51107081, 51477096) and the State Key Laboratory of Power System in Tsinghua University under Grant SKLD13KZ02 for finical support. P.K.J. and X.Y.H. thank the National Natural Science Foundation of China (No. 51277117) and the Special Fund of the National Priority Basic Research of China under Grant 2014CB239503 for financial support.

■ REFERENCES

(1) Huang, X. Y.; Jiang, P. K. Core-Shell Structured High-k Polymer Nanocomposites for Energy Storage and Dielectric Applications. *Adv. Mater.* **2014**, DOI: 10.1002/adma.201401310.

(2) Zhu, L.; Wang, Q. Novel Ferroelectric Polymers for High Energy Density and Low Loss Dielectrics. *Macromolecules* **2012**, *45*, 2937−2954.

(3) Dang, Z. M.; Yuan, J. K.; Zha, J. W.; Zhou, T.; Li, S. T.; Hu, G. H. Fundamentals, Processes and Applications of High-permittivity Polymer Matrix Composites. *Prog. Mater. Sci.* **2012**, *57*, 660−723.

(4) Hardy, C. G.; Islam, M. S.; Gonzalez-Delozier, D.; Morgan, J. E.; Cash, B.; Benicewicz, B. C.; Ploehn, H. J.; Tang, C. B. Converting an Electrical Insulator into a Dielectric Capacitor: End-Capping Polystyrene with Oligoaniline. *Chem. Mater.* **2013**, *25*, 799−807.

(5) Chu, B. J.; Zhou, X.; Ren, K. L.; Neese, B.; Lin, M. R.; Wang, Q.; Bauer, F.; Zhang, Q. M. A Dielectric Polymer with High Electric Energy Density and Fast Discharge Speed. *Science* **2006**, *313*, 334−336.

(6) Dang, Z. M.; Yuan, J. K.; Yao, S. H.; Liao, R. J. Flexible Nanodielectric Materials with High Permittivity for Power Energy Storage. *Adv. Mater.* **2013**, *25*, 6334−6365.

(7) Li, Z.; Fredin, L. A.; Tewari, P.; DiBenedetto, S. A.; Lanagan, M. T.; Ratner, M. A.; Marks, T. J. In Situ Catalytic Encapsulation of Core-Shell Nanoparticles Having Variable Shell Thickness: Dielectric and Energy Storage Properties of High-Permittivity Metal Oxide Nanocomposites. *Chem. Mater.* **2010**, *22*, 5154−5164.

(8) Li, J.; Claude, J.; Norena-Franco, L.; Seok, S.; Wang, Q. Electrical Energy Storage in Ferroelectric Polymer Nanocomposites Containing Surface-functionalized $BaTiO_3$ Nanoparticles. *Chem. Mater.* **2008**, *20*, 6304−6306.

(9) Jung, H. M.; Kang, J. H.; Yang, S. Y.; Won, J. C.; Kim, Y. S. Barium Titanate Nanoparticles with Diblock Copolymer Shielding Layers for High-Energy Density Nanocomposites. *Chem. Mater.* **2010**, *22*, 450−456.

(10) Guo, N.; DiBenedetto, S. A.; Tewari, P.; Lanagan, M. T.; Ratner, M. A.; Marks, T. J. Nanoparticle, Size, Shape, and Interfacial Effects on Leakage Current Density, Permittivity, and Breakdown Strength of Metal Oxide-Polyolefin Nanocomposites: Experiment and Theory. *Chem. Mater.* **2010**, *22*, 1567−1578.

(11) Chon, J.; Ye, S.; Cha, K. J.; Lee, S. C.; Koo, Y. S.; Jung, J. H.; Kwon, Y. K. High-K Dielectric Sol-Gel Hybrid Materials Containing Barium Titanate Nanoparticles. *Chem. Mater.* **2010**, *22*, 5445−5452.

(12) Guo, M.; Hayakawa, T.; Kakimoto, M.; Goodson, T. Organic Macromolecular High Dielectric Constant Materials: Synthesis, Characterization, and Applications. *J. Phys. Chem. B* **2011**, *115*, 13419−13432.

(13) Rahimabady, M.; Mirshekarloo, M. S.; Yao, K.; Lu, L. Dielectric Behaviors and High Energy Storage Density of Nanocomposites with Core-shell $BaTiO_3$@TiO_2 in Poly(vinylidene fluoride-hexafluoropropylene). *Phys. Chem. Chem. Phys.* **2013**, *15*, 16242−16248.

(14) Tang, H.; Lin, Y.; Sodano, H. A. Synthesis of High Aspect Ratio $BaTiO_3$ Nanowires for High Energy Density Nanocomposite Capacitors. *Adv. Energy Mater.* **2013**, *3*, 451−456.

(15) Tang, H.; Sodano, H. A. Ultra High Energy Density Nanocomposite Capacitors with Fast Discharge Using $Ba_{0.2}Sr_{0.8}TiO_3$ Nanowires. *Nano Lett.* **2013**, *13*, 1373−1379.

(16) Tomer, V.; Polizos, G.; Manias, E.; Randall, C. A. Epoxy-based Nanocomposites for Electrical Energy Storage. I: Effects of Montmorillonite and Barium Titanate Nanofillers. *J. Appl. Phys.* **2010**, *108*, 074116.

(17) Wu, W.; Huang, X. Y.; Li, S. T.; Jiang, P. K.; Toshikatsu, T. Novel Three-Dimensional Zinc Oxide Superstructures for High Dielectric Constant Polymer Composites Capable of Withstanding High Electric Field. *J. Phys. Chem. C* **2012**, *116*, 24887−24895.

(18) Siddabattuni, S.; Schuman, T. P.; Dogan, F. Dielectric Properties of Polymer-Particle Nanocomposites Influenced by Electronic Nature of Filler Surfaces. *ACS Appl. Mater. Interfaces* **2013**, *5*, 1917−1927.

(19) Zhou, T.; Zha, J. W.; Cui, R. Y.; Fan, B. H.; Yuan, J. K.; Dang, Z. M. Improving Dielectric Properties of $BaTiO_3$/Ferroelectric Polymer Composites by Employing Surface Hydroxylated BaTiO3 Nanoparticles. *ACS Appl. Mater. Interfaces* **2011**, *3*, 2184−2188.

(20) Kim, P.; Doss, N. M.; Tillotson, J. P.; Hotchkiss, P. J.; Pan, M. J.; Marder, S. R.; Li, J. Y.; Calame, J. P.; Perry, J. W. High Energy Density Nanocomposites Based on Surface-Modified $BaTiO_3$ and a Ferroelectric Polymer. *ACS Nano* **2009**, *3*, 2581−2592.

(21) Kim, P.; Jones, S.; Hotchkiss, P.; Haddock, J.; Kippelen, B.; Marder, S.; Perry, J. Phosphonic Acid Modified Barium Titanate Polymer Nanocomposites with High Permittivity and Dielectric Strength. *Adv. Mater.* **2007**, *19*, 1001−1005.

(22) Shen, Y.; Lin, Y. H.; Nan, C. W. Interfacial Effect on Dielectric Properties of Polymer Nanocomposites Filled with Core/shell-structured Particles. *Adv. Funct. Mater.* **2007**, *17*, 2405−2410.

(23) Yu, K.; Niu, Y. J.; Bai, Y. Y.; Zhou, Y. C.; Wang, H. Poly(vinylidene fluoride) Polymer Based Nanocomposites with Significantly Reduced Energy Loss by Filling with Core-shell

Structured $BaTiO_3/SiO_2$ Nanoparticles. *Appl. Phys. Lett.* **2013**, *102*, 102903.

(24) Almadhoun, M. N.; Bhansali, U. S.; Alshareef, H. N. Nanocomposites of ferroelectric polymers with surface-hydroxylated $BaTiO_3$ nanoparticles for energy storage applications. *J. Mater. Chem.* **2012**, *22*, 11196−11200.

(25) Huang, X. Y.; Xie, L. Y.; Yang, K.; Wu, C.; Jiang, P. K.; Li, S. T.; Wu, S.; Tatsumi, K.; Tanaka, T. Role of Interface in Highly Filled Epoxy/$BaTiO_3$ Nanocomposites. Part II- Effect of Nanoparticle Surface Chemistry on on Processing, Thermal Expansion, Energy Storage and Breakdown Strength of the Nanocomposites. *IEEE Trans. Dielectr. Electr. Insul.* **2014**, *21*, 480−487.

(26) Song, Y.; Shen, Y.; Liu, H. Y.; Lin, Y. H.; Li, M.; Nan, C. W. Improving the Dielectric Constants and Breakdown Strength of Polymer Composites: Effects of the Shape of the $BaTiO_3$ Nanoinclusions, Surface Modification and Polymer Matrix. *J. Mater. Chem.* **2012**, *22*, 16491−16498.

(27) Paniagua, S. A.; Kim, Y.; Henry, K.; Kumar, R.; Perry, J. W.; Marder, S. R. Surface-Initiated Polymerization from Barium Titanate Nanoparticles for Hybrid Dielectric Capacitors. *ACS Appl. Mater. Interfaces* **2014**, *6*, 3477−3482.

(28) Fredin, L. A.; Li, Z.; Lanagan, M. T.; Ratner, M. A.; Marks, T. J. Sustainable High Capacitance at High Frequencies: Metallic Aluminum - Polypropylene Nanocomposites. *ACS Nano* **2013**, *7*, 396−407.

(29) Fredin, L. A.; Li, Z.; Lanagan, M. T.; Ratner, M. A.; Marks, T. J. Substantial Recoverable Energy Storage in Percolative Metallic Aluminum-Polypropylene Nanocomposites. *Adv. Funct. Mater.* **2013**, *23*, 3560−3569.

(30) Fredin, L. A.; Li, Z.; Ratner, M. A.; Lanagan, M. T.; Marks, T. J. Enhanced Energy Storage and Suppressed Dielectric Loss in Oxide Core-Shell-Polyolefin Nanocomposites by Moderating Internal Surface Area and Increasing Shell Thickness. *Adv. Mater.* **2012**, *24*, 5946−5953.

(31) Tchoul, M. N.; Fillery, S. P.; Koerner, H.; Drummy, L. F.; Oyerokun, F. T.; Mirau, P. A.; Durstock, M. F.; Vaia, R. A. Assemblies of Titanium Dioxide-Polystyrene Hybrid Nanoparticles for Dielectric Applications. *Chem. Mater.* **2010**, *22*, 1749−1759.

(32) Xie, L. Y.; Huang, X. Y.; Huang, Y. H.; Yang, K.; Jiang, P. K. Core-shell Structured Hyperbranched Aromatic Polyamide/$BaTiO_3$ Hybrid Filler for Poly(vinylidene fluoride-trifluoroethylene-chlorofluoroethylene) Nanocomposites with the Dielectric Constant Comparable to That of Percolative Composites. *ACS Appl. Mater. Interfaces* **2013**, *5*, 1747−1756.

(33) Xie, L. Y.; Huang, X. Y.; Huang, Y. H.; Yang, K.; Jiang, P. K. Core@Double-Shell Structured $BaTiO_3$-Polymer Nanocomposites with High Dielectric Constant and Low Dielectric Loss for Energy Storage Application. *J. Phys. Chem. C* **2013**, *117*, 22525−22537.

(34) Xie, L. Y.; Huang, X. Y.; Wu, C.; Jiang, P. K. Core-shell Structured Poly(methyl methacrylate)/$BaTiO_3$ Nanocomposites Prepared by in situ Atom Tansfer Radical Polymerization: a Route to High Dielectric Constant Materials with the Inherent Low Loss of the Base Polymer. *J. Mater. Chem.* **2011**, *21*, 5897−5906.

(35) Xie, L. Y.; Huang, X. Y.; Yang, K.; Li, S. T.; Jiang, P. K. "Grafting to" Route to PVDF-HFP-GMA/$BaTiO_3$ Nanocomposites with High Dielectric Constant and High Thermal Conductivity for Energy Storage and Thermal Management Applications. *J. Mater. Chem. A* **2014**, *2*, 5244−5251.

(36) Yang, K.; Huang, X.; Huang, Y.; Xie, L.; Jiang, P. Fluoro-Polymer@$BaTiO_3$ Hybrid Nanoparticles Prepared via RAFT Polymerization: Toward Ferroelectric Polymer Nanocomposites with High Dielectric Constant and Low Dielectric Loss for Energy Storage Application. *Chem. Mater.* **2013**, *25*, 2327−2338.

(37) Yang, K.; Huang, X. Y.; Xie, L. Y.; Wu, C.; Jiang, P. K.; Tanaka, T. Core-Shell Structured Polystyrene/$BaTiO_3$ Hybrid Nanodielectrics Prepared by In Situ RAFT Polymerization: A Route to High Dielectric Constant and Low Loss Materials with Weak Frequency Dependence. *Macromol. Rapid Commun.* **2012**, *33*, 1921−1926.

(38) Yang, K.; Huang, X. Y.; Zhu, M.; Xie, L. Y.; Tanaka, T.; Jiang, P. K. Combining RAFT Polymerization and Thiol-Ene Click Reaction for Core-Shell Structured Polymer@$BaTiO_3$ Nanodielectrics with High Dielectric Constant, Low Dielectric Loss, and High Energy Storage Capability. *ACS Appl. Mater. Interfaces* **2014**, *6*, 1812−1822.

(39) Lai, J. T.; Filla, D.; Shea, R. Functional Polymers from Novel Carboxyl-Terminated Trithiocarbonates as Highly Efficient RAFT Agents. *Macromolecules* **2002**, *35*, 6754−6756.

(40) Zhang, X. Q.; Li, J. G.; Li, W.; Zhang, A. F. Synthesis and Characterization of Thermo- and pH-Responsive Double-Hydrophilic Diblock Copolypeptides. *Biomacromolecules* **2007**, *8*, 3557−3567.

(41) Nishi, T.; Wang, T. T. Melting Point Depression and Kinetic Effects of Cooling on Crystallization in Poly(vinylidene fluoride)-Poly(methyl methacrylate) Mixtures. *Macromolecules* **1975**, *8*, 909−915.

(42) Martins, P.; Lopes, A. C.; Lanceros-Mendez, S. Electroactive Phases of Poly(vinylidene fluoride): Determination, Processing and Applications. *Prog. Polym. Sci.* **2014**, *39*, 683−706.

(43) Huang, X. Y.; Jiang, P. K.; Kim, C.; Liu, F.; Yin, Y. Influence of Aspect Ratio of Carbon Nanotubes on Crystalline Phases and Dielectric Properties of Poly(vinylidene fluoride). *Eur. Polym. J.* **2009**, *45*, 377−386.

(44) Huang, X. Y.; Zhi, C. Y.; Jiang, P. K.; Golberg, D.; Bando, Y.; Tanaka, T. Temperature-Dependent Electrical Property Transition of Graphene Oxide Paper. *Nanotechnology* **2012**, *23*, 455705.

(45) Schönhals, A.; Kremer, F. Analysis of Dielectric Spectra. In *Broadband Dielectric Spectroscopy*; Kremer, F., Schönhals, A., Eds.; Springer-Verlag: Berlin Heidelberg GmbH, 2002; p 729.

(46) Ku, C. C.; Liepins, R. *Electrical Properties of Polymers – Chemical Principles*; Publishers: Munich, 1987.

(47) Huang, X. Y.; Xie, L. Y.; Jiang, P. K.; Wang, G. L.; Liu, F. Electrical, Thermophysical and Micromechanical Properties of Ethylene-vinyl Acetate Elastomer Composites with Surface Modified $BaTiO_3$ Nanoparticles. *J. Phys. D Appl. Phys.* **2009**, *42*, 245407.

(48) Huang, X. Y.; Xie, L. Y.; Hu, Z. W.; Jiang, P. K. Influence of $BaTiO_3$ Nanoparticles on Dielectric, Thermophysical and Mechanical Properties of Ethylene-Vinyl Acetate Elastomer/BaTiO3Microcomposites. *IEEE Trans. Dielectr. Electr. Insul.* **2011**, *18*, 375−383.

(49) Emmert, S.; Wolf, M.; Gulich, R.; Krohns, S.; Kastner, S.; Lunkenheimer, P.; Loidl, A. Electrode Polarization Effects in Broadband Dielectric Spectroscopy. *Eur. Phys. J. B* **2011**, *83*, 157−165.

(50) Tomer, V.; Polizos, G.; Randall, C. A.; Manias, E. Polyethylene Nanocomposite Dielectrics: Implications of Nanofiller Orientation on High Field Properties and Energy Storage. *J. Appl. Phys.* **2011**, *109*, 3569696.

(51) Fukada, E. Recent Developments of Polar Piezoelectric Polymers. *IEEE Trans. Dielectr. Electr. Insul.* **2006**, *13*, 1110−1119.